Modeling particle formation during low-pressure silane oxidation: Detailed chemical kinetics and aerosol dynamics

S.-M. Suh, M. R. Zachariah,[a] and S. L. Girshick
Departments of Mechanical Engineering and Chemistry and the Supercomputing Institute, University of Minnesota, Minneapolis, Minnesota 55455

A detailed chemical kinetic model is presented for silicon oxide clustering that leads to particle nucleation during low-pressure silane oxidation. Quantum Rice–Ramsperger–Kassel theory was applied to an existing high-pressure silane oxidation mechanism to obtain estimates for the pressure dependence of rate parameters. Four classes of clustering pathways were considered based on current knowledge of reaction kinetics and cluster properties in the Si–H–O system. The species conservation equations and a moment-type aerosol dynamics model were formulated for a batch reactor undergoing homogeneous nucleation and particle growth by surface reactions and coagulation. The chemical kinetics model was coupled to the aerosol dynamics model, and time-dependent zero-dimensional simulations were conducted. The effects of pressure and temperature were examined, and the main contributing processes to particle formation and growth were assessed, for conditions around 0.8 Torr, 773 K, and an initial oxygen-to-silane ratio of 15. © *2001 American Vacuum Society.* [DOI: 10.1116/1.1355757]

I. INTRODUCTION

Low-pressure chemical vapor deposition (LPCVD) of SiO_2 films from silane and oxygen is widely used in microelectronics fabrication. SiO_2 is used in electronic components because of its insulating properties and as a barrier to impurity diffusion.[1]

During LPCVD film deposition rates are limited by the gas-phase nucleation of particles inside the reactor. Moreover, the generation of particles can be a significant source of product defects and yield loss. The critical diameter of ''killer particles,'' defined as one third to one half of the gate length, is projected to shrink below about 50 nm by 2003, and below about 20 nm by 2012.[2] Homogeneous gas-phase nucleation can play a dominant role in generating these small particles. Fundamental understanding of particle nucleation, growth and transport is crucial not only to optimizing operating parameters but also to obtaining desired film properties.

Silane oxidation has been the subject of considerable study since the investigation of the explosive nature of silane and oxygen mixtures by Emeleus and Stewart.[3] While there are still many uncertainties in the reaction kinetics due to the complexity of Si–H–O chemistry, a growing body of work enables reasonable estimates of rate parameters. Based on previously reported mechanisms for silane oxidation and pyrolysis, Babushok *et al.*[4] recently proposed a relatively complete mechanism and made comparisons with experimental data on the critical conditions for chain ignition over a wide range of temperatures at atmospheric pressure. Meeks *et al.*[5] proposed a surface chemistry mechanism to simulate film growth by utilizing empirical calculations and data obtained from tetraethoxysilane (TEOS) CVD experiments. Based on this body of recent work it is now possible to obtain reason-able predictions of SiO_2 film growth rates under conditions typical of LPCVD.

In an experimental study on particle formation during LPCVD of SiO_2 films, Liehr and Cohen[6] identified powder formation or ''snow'' regions as a function of temperature and pressure in their multichamber reactor. They further deduced that the generation of $SiOH_x$ species from fast gas-phase reactions can significantly degrade film quality. Based on their data we selected a base set of operating conditions that lies on the boundary between particle-free film growth and strong gas-phase nucleation: an initial oxygen-to-silane molar ratio of $R = 15$, pressure $p = 0.8$ Torr (107 Pa) and temperature $T = 773$ K.

Recently Swihart and Girshick[7] presented a detailed kinetic mechanism for gas-phase nucleation of hydrogenated silicon particles for the relatively simpler problem of thermal decomposition of silane, in the absence of oxygen, and this mechanism was coupled to a moment-type aerosol dynamics model[8] to predict particle growth, coagulation and transport for conditions typical of CVD of amorphous silicon films. There have been several previous attempts[9–11] to model particle formation in the more complex Si–H–O system. These models simplified the treatment of nucleation either by employing a highly simplified global reaction set and/or by utilizing classical nucleation theory.

A few theoretical studies have been conducted regarding the thermochemistry of the smallest clusters in the silane–oxygen system. Kudo and Nagase[12] calculated heats of formation of SiH_2O clusters up to the tetramer. Zachariah and Tsang[13,14] applied *ab initio* molecular orbital theories in conjunction with reaction rate theory to obtain thermochemistry, energetics and kinetics for a number of $Si_xH_yO_z$ reactions and SiO clustering reactions up to the tetramer. More recently Nayak *et al.*[15] reported *ab initio* calculations of SiO_2 clusters containing up to six silicon atoms.

[a]Electronic mail: mrz@me.umn.edu

In this work we have developed a detailed mechanism for silicon oxide clustering leading to particle nucleation during silane oxidation. Thermochemical properties of silicon oxide clusters and their reaction parameters were estimated using data obtained from *ab initio* calculations together with statistical mechanical formulations. This clustering mechanism was coupled to a moment-type aerosol dynamics model. In Secs. II–IV we present details of the chemical kinetics model, conservation equations for a batch reactor, and an aerosol dynamics model. In Sec. V we present results of time-dependent simulations for a batch reactor.

II. CHEMICAL KINETICS

Our base gas-phase silane oxidation mechanism is based primarily on the work of Babushok et al.,[4] which was developed to study self-ignition and flame propagation properties of silane combustion systems at atmospheric pressure. Babushok et al. compiled previously suggested mechanisms for silane oxidation and pyrolysis, and adjusted reaction parameters to take into account recent experimental and theoretical studies over a wide temperature range (300–2000 K). To complete the reaction pathways for intermediate species, we also included a number of reactions of $Si_xH_yO_z$ species proposed by Zachariah and Tsang.[14]

A. Quantum Rice–Ramsperger–Kassel theory

The Babushok et al.[4] and Zachariah and Tsang[14] rate parameters were determined for atmospheric-pressure conditions, while our primary interest lies in the 1 Torr regime. Because the role of highly reactive radicals such as H, OH and O in chain-branching steps is crucial to the Si–H–O

system, careful treatment of the pressure dependence of rate parameters is necessary. We applied quantum Rice–Ramsperger–Kassel (QRRK) theory[16–18] to the base mechanism to evaluate the pressure dependence of 19 unimolecular reactions whose activation energies are known.[14] The major advantage of QRRK theory over the more sophisticated Rice–Ramsperger–Kassel–Marcus (RRKM) theory[19] is a substantial simplification of the input data required. In particular, a geometric mean vibrational frequency is used rather than all the vibrational frequencies for the decomposing reactant. This simplification predicts fall-off curves with reasonable accuracy in most situations as long as the rate constant $k \geq 10^{-4}\,s^{-1}$.[16,20] A detailed description of the application of QRRK theory can be found in Ref. 16.

Implementation of QRRK theory requires geometric mean vibrational frequencies, high-pressure-limit preexponential factors, activation energies and Lennard-Jones transport properties. For the 19 unimolecular reactions considered, we assumed temperature-independent recombination rate coefficients to be $2 \times 10^{13}\,cm^3\,mol^{-1}\,s^{-1}$ following the generic rate coefficients of Dean.[16] The high-pressure-limit preexponential factors in the reverse direction were then computed from the equilibrium constants and the known activation energies. The geometric mean vibrational frequencies and Lennard-Jones transport properties, including collision diameters, were estimated based on the results of *ab initio* calculations by Zachariah and Tsang.[14] Table I summarizes the rate parameters of the reactions at 1 atm and the correction factors, $k/k_{1\,atm}$, at 0.8 Torr calculated using QRRK theory.

TABLE I. Rate parameters for unimolecular reactions at 1 atm and the rate correction factors determined using QRRK theory at 0.8 Torr. Forward rate constants are expressed in the form of $k_f = (k/k_{1\,atm})AT^{\beta} \times \exp(-E_a/RT)$.

Reaction		A (cm^3 mol s)	β	E_a (cal/mol)	$k/k_{1\,atm}$	Note(s)
1	$SiH_2O+H \leftrightarrow SiH_2OH$	$6.50E+24$	-3.6	8230	$1.0E-3$	a,b
2	$SiH_3O+H \leftrightarrow SiH_3OH$	$1.23E+16$	0.5	160	1.0	a,b
3	$SiH_2+H_2O \leftrightarrow SiH_3OH$	$2.80E+31$	-6.4	16 140	$1.0E-3$	a,b
4	$H+SiO_2 \leftrightarrow SiOOH$	$8.50E+24$	-4.0	5660	$1.0E-3$	a,b
5	$SiO+OH \leftrightarrow SiOOH$	$2.10E+23$	-3.6	1900	$1.0E-3$	a,b
6	$HSiOH \leftrightarrow SiO+H_2$	$9.40E+28$	-3.8	38 550	$1.0E-3$	a,b
7	$SiH_2OH \leftrightarrow SiHO+H_2$	$9.60E+27$	-3.4	59 820	$1.0E-3$	a,b
8	$SiH_3OH \leftrightarrow SiH_2O+H_2$	$2.01E+27$	-4.3	68 160	$3.0E-3$	a,b
9	$SiH_3OH \leftrightarrow HSiOH+H_2$	$2.20E+26$	-4.2	66 570	$2.8E-3$	a,b
10	$Si_2H_4 \leftrightarrow SiH_2+SiH_2$	$1.00E+16$	0	59 000	$1.0E-3$	a
11	$Si_2H_4 \leftrightarrow Si_2H_2+H_2$	$3.00E+16$	0	34 990	$1.0E-3$	a
12	$Si_2H_5 \leftrightarrow Si_2H_3+H_2$	$3.16E+14$	0	53 000	$3.8E-2$	a
13	$SiH_3O_2 \leftrightarrow SiH_2O+OH$	$8.6E+14$	0	40 000	$1.0E-3$	a
14	$SiH_3O_2H \leftrightarrow SiH_3O+OH$	$6.50E+14$	0	48 700	$7.2E-3$	a
15	$HSiOOH \leftrightarrow SiOOH+H$	$5.00E+14$	0	90 000	$2.7E-3$	a
16	$HSiOOH \leftrightarrow SiO_2+H_2$	$1.00E+10$	0	54 000	$8.5E-1$	a
17	$SiH_2O \leftrightarrow SiO+H_2$	$1.00E+12$	0	60 800	$1.0E-2$	a
18	$2HSiOOH \leftrightarrow (HSiOOH)_2$	$1.70E+49$	-9.6	12 300	1.0	b
19	$2SiH_2O \leftrightarrow (SiH_2O)_2$	$3.60E+38$	-6.8	11 227	1.0	b

[a]Reference 4.
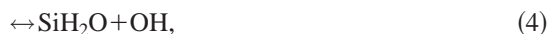[b]High-pressure-limit rate parameters are found in Ref. 14.

B. Base gas-phase mechanism

Our base kinetic mechanism consists of 36 gas species undergoing 221 reactions. In an oxidizing environment thermal decomposition of silane is negligible, and silylene, which is the dominant reactive species formed under thermal conditions, is only a minor contributor. Silylene is formed by the reaction

$$SiH_4 + M \leftrightarrow SiH_2 + H_2 + M, \tag{1}$$
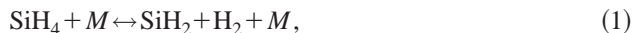
where M denotes a third body.

Instead direct interaction between silane and oxygen initiates the production of SiH_3, which then reacts with oxygen to produce an activated compound, $SiH_3O_2^*$, which then decomposes to produce three primary chain carriers, H, OH and O through reactions (3)–(7):

$$SiH_3 + O_2 \leftrightarrow SiH_3O_2^*, \tag{2}$$

$$SiH_3O_2^* \leftrightarrow SiOOH + 2H, \tag{3}$$

$$\leftrightarrow SiH_2O + OH, \tag{4}$$

$$\leftrightarrow SiH_3O + O, \tag{5}$$

$$\leftrightarrow SiO + H_2O + H, \tag{6}$$

$$\leftrightarrow HSiOOH + H. \tag{7}$$

These chain carriers in turn participate in the destruction of silane or in chain-terminating reactions. The competition between the branching and the terminating steps determines the explosion limits at a given temperature and pressure. Whereas silane pyrolysis leading to particle formation under nonoxidizing conditions is overall an endothermic process, silane oxidation to silica is extremely exothermic. The pyrophoricity of silane arises from the rapidity of the chain-branching steps, reactions (3)–(7), which have zero activation energy.

There exist large discrepancies in the reported activation energies for the reaction $SiO + O_2 \leftrightarrow SiO_2 + O$. Britten et al.[21] used a value of 6.5 kcal/mol, which is lower than the 15 kcal/mol heat of reaction that we used in this study. Babushok et al.[4] used 30 kcal/mol, while our ab initio calculations indicate that it could be as high as 61 kcal/mol. In the future more attention should be focused on this chain-propagating reaction, especially for low temperatures, where a lower activation energy would cause substantial production of atomic oxygen, which provides an additional chain-branching step. In addition, as this reaction opens a conversion route from SiO to SiO_2, it plays an important role in particle surface growth and clustering reactions, discussed below.

Figures 1 and 2 show results obtained with the gas-phase mechanism at the base operating condition. For these calculations we utilized the SENKIN software module,[22] which is one of the CHEMKIN family of codes designed for time-dependent chemical kinetics calculations. Figure 1 shows the dominant reaction pathway based on an integration over 10 s of reaction time. As discussed above, SiH_3 lies at the core from which the reaction network propagates. The five chain
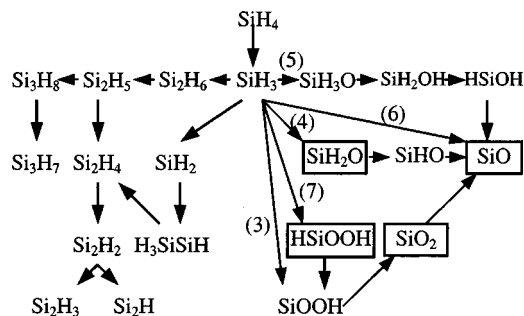

FIG. 1. Reaction pathways of gas species at 0.8 Torr, 773 K and $R = 15$. The species in boxes showed the highest concentrations in the batch reactor simulation presented in Fig. 2. Numbers in parentheses correspond to reaction numbers in the text.

reaction routes, reactions (3)–(7), dominate the chemistry, leading to the production of SiO and SiO_2 via several intermediate species. The silicon hydride network shown on the left half of the diagram indicates that, unlike what would be expected under nonoxidizing conditions,[23] silane does not directly create SiH_2 in this system. The formation of silicon hydrides with two or three silicon atoms through reactions with H, OH and O behaves like a radical scavenging process.

In Fig. 2 we plot the computed gas-phase species mole fractions as a function of time for those species with mole fractions greater than 1 ppm. We note that SiO, SiO_2, SiH_2O and HSiOOH are predicted to be the most abundant silicon-containing products of silane decomposition. These four species were identified as the most probable nucleating species by Zachariah and Tsang in previous studies.[13,14]

C. Chemical clustering mechanism

The kinetics of nucleation were modeled by a chemical clustering approach based on the detailed gas-phase chemistry. Considering the complexity inherent in the Si–H–O system, a mechanism that would include all possible species would be unrealistically large. Our approach is to assume that the species most likely to contribute the dominant frac-
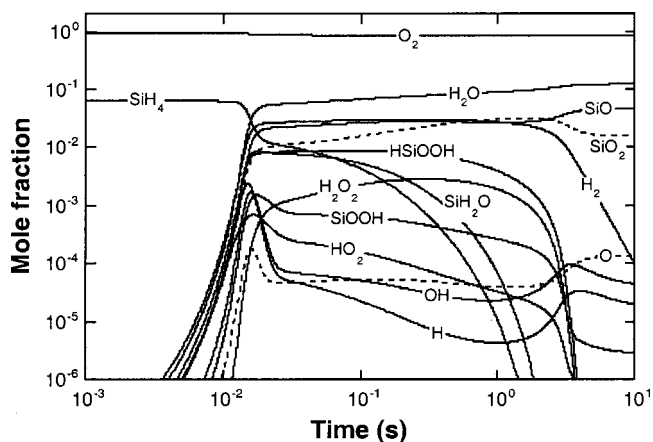

FIG. 2. Predicted evolution of gas composition at 0.8 Torr, 773 K and $R = 15$ for a batch reactor.

tion of the nucleating mass are those silicon-containing species that are produced in the highest concentrations.

Among the four most abundant species mentioned above, we considered, first, the reversible self-clustering of SiO and SiO_2 as expressed in reactions (8) and (9). Our choice of these two species is mostly attributable to the following reasons.

(1) Figure 2 shows that SiO and SiO_2 are two of the most abundant silicon-containing species. (2) *Ab initio* data are available only for a limited number of these clusters. (3) As it is highly probable that polymerization and insertion during the self-clustering of SiO and SiO_2 clusters occur without a potential barrier,[13,14] we can estimate the rate parameters of the clustering reactions,

$$(SiO)_n + SiO \leftrightarrow (SiO)_{n+1}, \tag{8}$$

$$(SiO_2)_n + SiO_2 \leftrightarrow (SiO_2)_{n+1}, \tag{9}$$
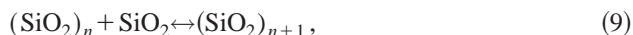
for $1 \leq n \leq 9$.

Second, we included the contribution of SiH_2O and HSiOOH and of their dimers through the two classes of irreversible reactions given in reactions (10) and (11). Based on the similarities of the ground-state molecular structures of the monomer and the dimer, comparing SiH_2O to SiO and HSiOOH to SiO_2,[14] the insertions of SiH_2O and HSiOOH and of their dimers into SiO and SiO_2 clusters, respectively, were assumed to be barrierless. The following dehydrogenation reactions were thus assumed to occur and to be barrierless:

$$(SiO)_n + (SiH_2O)_m \rightarrow (SiO)_{n+m} + mH_2, \tag{10}$$

$$(SiO_2)_n + (HSiOOH)_m \rightarrow (SiO_2)_{n+m} + mH_2, \tag{11}$$
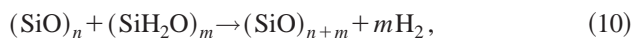
for $1 \leq n \leq 9$ and $m = 1$ or 2.

We did not consider the other clustering pathways such as the cross clustering between SiO and SiO_2 clusters since including all the possibilities will be neither practical nor helpful in gaining further accuracy and reliability of the model with the current understanding in this system. Moreover, the consideration of additional clustering pathways would not change the results significantly especially for the particle dynamics since we expect that the mass flux from gas clusters to particles will remain relatively unaffected so long as we have suitable pathways.

Clusters containing more than 10 silicon atoms, $(SiO)_{11}$, $(SiO_2)_{11}$, $(SiO)_{12}$ and $(SiO_2)_{12}$, were assumed to form irreversibly, and the nucleation rate was obtained from the sum of their production rates.

1. Thermochemistry of silicon oxide clusters

Ab initio calculations for SiO clusters up to the tetramer were performed by Zachariah and Tsang,[13] while the corresponding results for SiO_2 clusters were reported by Nayak *et al.*,[15] who also provided us with their unpublished vibrational frequencies, zero-point energies and moments of inertia. These data sets for ground-state clusters were used to compute enthalpies and entropies derived by standard statistical mechanics methods.[24]
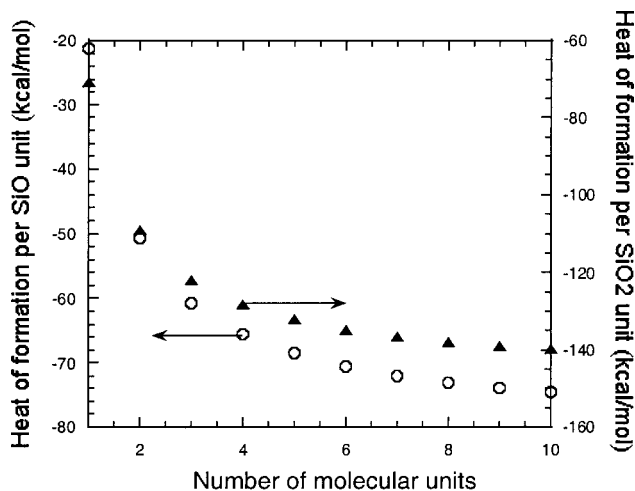

FIG. 3. Calculated standard heats of formation per molecular unit of SiO and SiO_2 clusters.

A linear least-squares fit on the smaller oxide clusters was used to provide extrapolated estimates of larger clusters containing up to 10 silicon atoms. The results were checked by comparing the calculated standard heats of formation of these clusters with the known values for the bulk condensed phase. Figure 3 shows that, although the sizes of clusters considered are very small, the standard heats of formation per molecular unit for SiO and SiO_2 clusters asymptotically approach the values of their condensed phases, 85 and 145 kcal/mol, respectively.

The thermochemical properties of SiO and SiO_2 clusters were expressed in terms of polynomial fitting coefficients in the standard NASA format used in the CHEMKIN family of codes.[25] The fitting coefficients are presented in the Appendix.

2. Rate parameters

To estimate the pressure-dependent rate constants of the four classes of clustering steps, reactions (8)–(11), we followed the same procedure described above, i.e., the use of generic recombination rate constants and QRRK theory.

We used temperature-independent high-pressure-limit recombination rate constants of 2×10^{13} $cm^3 mol^{-1} s^{-1}$ for dimerization and trimerization ($n = 1,2$), 3×10^{13} $cm^3 mol^{-1} s^{-1}$ for formation of the tetramer ($n = 3$), and 1×10^{14} $cm^3 mol^{-1} s^{-1}$ for the higher polymerization steps ($n \geq 4$). As the self-clustering of SiO and SiO_2 clusters occurs without a potential barrier,[14] we assumed the activation energies of the dissociation reactions to be temperature independent and equal to the corresponding heats of reaction at 773 K. The high-pressure-limit pre-exponential factors were then obtained from the equilibrium constants and the activation energies. The other input parameters to QRRK theory, including vibrational frequencies and collision diameters, were estimated based on the work of Zachariah and Tsang[14] and of Nayak *et al.*[15] for SiO and SiO_2 clusters, respectively. The same pressure dependence of self-clustering reactions (8) and (9) was used for SiH_2O and HSiOOH insertion reactions

TABLE II. Clustering reactions considered and rate parameters at 0.8 Torr estimated by QRRK theory. Forward rate constants are expressed in the form of $k_f = (k/k_\infty) A_\infty \exp(-E_a/RT)$.

	Reaction	A_∞ (cm^3 mol s)	E_a (cal/mol)	k/k_∞	Note
SiO self-clustering					
1	$(SiO)_2 \leftrightarrow SiO + SiO$	1.04E+15	49 580	5.0E−4	a
2	$(SiO)_3 \leftrightarrow (SiO)_2 + SiO$	3.78E+15	53 160	1.9E−2	a
3	$(SiO)_4 \leftrightarrow (SiO)_3 + SiO$	1.49E+14	36 670	9.3E−2	a
4	$(SiO)_5 \leftrightarrow (SiO)_4 + SiO$	2.73E+14	51 020	5.9E−1	a
5	$(SiO)_6 \leftrightarrow (SiO)_5 + SiO$	2.88E+14	46 920	6.9E−1	a
6	$(SiO)_7 \leftrightarrow (SiO)_6 + SiO$	2.88E+14	46 920	8.3E−1	a
7	$(SiO)_8 \leftrightarrow (SiO)_7 + SiO$	2.88E+14	46 900	9.1E−1	a
8	$(SiO)_9 \leftrightarrow (SiO)_8 + SiO$	2.88E+14	46 950	9.8E−1	a
9	$(SiO)_{10} \leftrightarrow (SiO)_9 + SiO$	2.88E+14	46 920	9.8E−1	a
Irreversible SiO clustering by $(SiH_2O)_m$, where $m=1$ or 2					
10	$SiO + (SiH_2O)_m \rightarrow (SiO)_{m+1} + mH_2$	2.00E+13	0	5.0E−4	
11	$(SiO)_2 + (SiH_2O)_m \rightarrow (SiO)_{m+2} + mH_2$	2.00E+13	0	1.9E−2	
12	$(SiO)_3 + (SiH_2O)_m \rightarrow (SiO)_{m+3} + mH_2$	3.00E+13	0	9.3E−2	
13	$(SiO)_4 + (SiH_2O)_m \rightarrow (SiO)_{m+4} + mH_2$	1.00E+14	0	5.9E−1	
14	$(SiO)_5 + (SiH_2O)_m \rightarrow (SiO)_{m+5} + mH_2$	1.00E+14	0	6.9E−1	
15	$(SiO)_6 + (SiH_2O)_m \rightarrow (SiO)_{m+6} + mH_2$	1.00E+14	0	8.3E−1	
16	$(SiO)_7 + (SiH_2O)_m \rightarrow (SiO)_{m+7} + mH_2$	1.00E+14	0	9.1E−1	
17	$(SiO)_8 + (SiH_2O)_m \rightarrow (SiO)_{m+8} + mH_2$	1.00E+14	0	9.8E−1	
18	$(SiO)_9 + SiH_2O \rightarrow (SiO)_{10} + H_2$	1.00E+14	0	9.8E−1	
19	$SiH_2O + (SiH_2O)_2 \rightarrow (SiO)_3 + 3H_2$	3.00E+13	0	9.3E−2	
SiO$_2$ self-clustering					
20	$(SiO_2)_2 \leftrightarrow SiO_2 + SiO_2$	1.91E+16	85 670	1.1E−1	a
21	$(SiO_2)_3 \leftrightarrow (SiO_2)_2 + SiO_2$	4.97E+17	95 810	5.9E−1	a
22	$(SiO_2)_4 \leftrightarrow (SiO_2)_3 + SiO_2$	1.25E+17	94 550	6.6E−1	a
23	$(SiO_2)_5 \leftrightarrow (SiO_2)_4 + SiO_2$	6.10E+17	94 780	6.6E−1	a
24	$(SiO_2)_6 \leftrightarrow (SiO_2)_5 + SiO_2$	5.78E+17	94 570	5.7E−1	a
25	$(SiO_2)_7 \leftrightarrow (SiO_2)_6 + SiO_2$	3.32E+17	92 050	1.0	a
26	$(SiO_2)_8 \leftrightarrow (SiO_2)_7 + SiO_2$	3.83E+17	93 530	8.7E−1	a
27	$(SiO_2)_9 \leftrightarrow (SiO_2)_8 + SiO_2$	3.33E+17	93 530	1.0	a
28	$(SiO_2)_{10} \leftrightarrow (SiO_2)_9 + SiO_2$	3.74E+17	93 530	8.9E−1	a
Irreversible SiO$_2$ clustering by $(HSiOOH)_m$, where $m=1$ or 2					
29	$SiO_2 + (HSiOOH)_m \rightarrow (SiO_2)_2 + mH_2$	2.00E+13	0	1.1E−1	
30	$(SiO_2)_2 + (HSiOOH)_m \rightarrow (SiO_2)_{m+2} + mH_2$	2.00E+13	0	5.9E−1	
31	$(SiO_2)_3 + (HSiOOH)_m \rightarrow (SiO_2)_{m+2} + mH_2$	3.00E+13	0	6.6E−1	
32	$(SiO_2)_4 + (HSiOOH)_m \rightarrow (SiO_2)_{m+2} + mH_2$	1.00E+14	0	6.6E−1	
33	$(SiO_2)_5 + (HSiOOH)_m \rightarrow (SiO_2)_{m+2} + mH_2$	1.00E+14	0	5.7E−1	
34	$(SiO_2)_6 + (HSiOOH)_m \rightarrow (SiO_2)_{m+2} + mH_2$	1.00E+14	0	1.0	
35	$(SiO_2)_7 + (HSiOOH)_m \rightarrow (SiO_2)_{m+2} + mH_2$	1.00E+14	0	8.7E−1	
36	$(SiO_2)_8 + (HSiOOH)_m \rightarrow (SiO_2)_{m+2} + mH_2$	1.00E+14	0	1.0	
37	$(SiO_2)_9 + HSiOOH \rightarrow (SiO_2)_{10} + H_2$	1.00E+14	0	8.9E−1	
38	$HSiOOH + (HSiOOH)_2 \rightarrow (SiO_2)_3 + 3H_2$	3.00E+13	0	5.9E−1	
Irreversible particle formation, where $n+m \geqslant 11$, $n=9$ or 10 and $m=1$ or 2					
39	$(SiO)_{10} + SiO \rightarrow particle$	1.60E+13	0.5	1.0	
40	$(SiO)_n + (SiH_2O)_m \rightarrow particle$	1.60E+13	0.5	1.0	
41	$(SiO_2)_{10} + SiO_2 \rightarrow particle$	1.60E+13	0.5	1.0	
42	$(SiO_2)_n + (HSiOOH)_m \rightarrow particle$	1.60E+13	0.5	1.0	

[a]Activation energy is assumed to be the enthalpy of reaction at 773 K.

(10) and (11), respectively. The resulting rate parameters at 0.8 Torr are summarized in Table II.

D. Surface growth mechanism

Single-particle growth occurs by heterogeneous chemistry on particle surfaces. We adopted as our base surface mecha-

nism the neutral chemistry portion of the surface reaction mechanism developed by Meeks et al.[5] to simulate film growth rates during low-pressure high-density plasma CVD of SiO$_2$ from silane, oxygen and argon gas mixtures. They estimated thermochemical data for surface species based on empirical methods using their results for the TEOS system, and obtained quantitative agreement between their calculated

film growth rates and their experimental results. Thirteen different surface species were defined, participating in 59 reactions. Eight gas-phase species were allowed to interact with surface sites to form bulk silicon dioxide.

This base mechanism was extended to include the deposition of clusters from the gas phase. SiO and SiO_2 clusters were assumed to deposit on particle surfaces to form bulk material with a sticking probability of unity. We assumed that the resulting surface mechanism is appropriate for describing the particle growth process, although the Meeks *et al.* mechanism was developed to model film growth on a flat substrate. We employed the formalism of the Surface Chemkin software[26] to implement the heterogeneous kinetics.

III. SPECIES CONSERVATION FOR A BATCH REACTOR WITH GAS-TO-PARTICLE CONVERSION

A. Zero-dimensional model: Batch reactor

We here adopt a zero-dimensional formulation, which is appropriate for systems whose behavior is dominated by chemical kinetics rather than by flow. The major advantage of such an approach is a large enhancement in computational efficiency, while still obtaining important insights into the system behavior. However it should be noted that, even where convective flow effects are negligible, actual reactors may have nonuniform temperature fields and other inhomogeneities, and that diffusion and particle thermophoresis can be important phenomena, especially at low pressures.

The mass conservation equation for each gas species was formulated for a batch reactor where particle formation occurs. The change of mass of the kth species can be expressed as

$$\frac{dm_k}{dt} = V\dot{w}_k^g W_k + V\dot{w}_k^n W_k + A\dot{s}_k W_k, \quad k=1,2,...,K_g, \quad (12)$$

where $\dot{w}_k^g$, $\dot{w}_k^n$ and $\dot{s}_k$ are the production rates of the kth gas species due to gas reaction, nucleation and surface reactions, respectively. W_k and m_k are, respectively, molecular weight and mass of the kth species. A is the area on which surface reactions can take place. V is the total volume of the gas. K_g is the total number of gas species.

The three terms on the right-hand side account for mass gain or loss of the kth species due to gas-phase reactions, particle nucleation and particle surface growth, respectively. After dividing Eq. (12) by $m=\rho V$, the total gas mass and applying the chain rule, we obtain

$$\rho\frac{dY_k}{dt} = -\frac{Y_k}{V}\frac{dm}{dt} + \left(\dot{w}_k^g + \dot{w}_k^n + \frac{A}{V}\dot{s}_k\right)W_k,$$

$$k=1,2,...,K_g, \quad (13)$$

where Y_k is the mass fraction of the kth species.

The total mass change of gas species due to particle surface reaction and nucleation can be written as

$$\frac{dm}{dt} = \sum_{k=1}^{K_g} A\dot{s}_k W_k + \sum_{k=1}^{K_g} V\dot{w}_k'' W_k. \quad (14)$$

Substituting Eq. (14) into Eq. (13), we obtain the equation of species mass continuity:

$$\rho\frac{dY_k}{dt} = -Y_k\left(\sum_{k=1}^{K_g}\frac{A}{V}\dot{s}_k W_k + \sum_{k=1}^{K_g}\dot{w}_k'' W_k\right)$$

$$+\left(\dot{w}_k^g + \dot{w}_k'' + \frac{A}{V}\dot{s}_k\right)W_k, \quad k$$

$$= 1,2,...,K_g. \quad (15)$$

To determine the particle surface-to-volume ratio, one needs to solve the aerosol general dynamic equation (GDE) together with Eq. (15).

The average mass density, ρ, can be obtained from the ideal gas law,

$$\rho = \frac{p\bar{W}}{RT}, \quad (16)$$

where $\bar{W}$ is the mean molecular weight of the gas mixture and R is the universal gas constant.

B. Surface species conservation

The concentration (or, equivalently, site fraction) of surface species needs to be calculated to obtain the species production rates, which are then used to predict rates of particle growth by surface reactions. The procedure corresponds to that of the gas-species mass conservation equation derived earlier.

Following the derivation presented by Coltrin *et al.*,[26] the change of moles of the kth surface species with time can be written as

$$\frac{dN_k}{dt} = A\dot{s}_k, \quad (17)$$

where N_k, the number of moles of the kth surface species, can be expressed in terms of site fraction, Z_k, site density, Γ, and the number of sites that the kth species occupies, Σ_k:

$$N_k = \frac{Z_k\Gamma A}{\Sigma_k}. \quad (18)$$

Substituting Eq. (18) into Eq. (17) and simplifying yields the surface species conservation equation in the form

$$\frac{dZ_k}{dt} = \frac{\dot{s}_k\Sigma_k}{\Gamma} - \frac{Z_k}{\Gamma}\frac{d\Gamma}{dt} - \frac{Z_k}{A}\frac{dA}{dt}. \quad (19)$$

Assuming that the total number of surface sites is conserved, the second term on the right-hand side drops out to yield

$$\frac{dZ_k}{dt} = \frac{\dot{s}_k\Sigma_k}{\Gamma} - \frac{Z_k}{A}\frac{dA}{dt}. \quad (20)$$

IV. AEROSOL DYNAMICS

To solve the aerosol GDE, which is a partial integrodifferential equation, the particle size distribution function must be represented in some mathematical form. Several approaches have been proposed to model the distribution func-

tion, including discrete, spline, sectional, discrete sectional and moment. The moment approach is one of the most computationally efficient methods, and is well suited for problems in which extensive chemical reactions are involved.[27]

In the moment method one solves for only the first few moments of the particle size distribution function, which is usually assumed to follow the general form of a lognormal function. These first few moments are directly related to the quantities that are usually of most interest, such as the total particle concentration, the mean particle size and the width of the size distribution.

A. Moment model for a batch reactor

The kth moment of the particle size distribution is defined by $M_k = \int_0^\infty v_p^k n(v_p,t) dv_p$, where v_p is particle volume and $n(v_p,t)$ is the particle size distribution function. Following the approach of Pratsinis and Kim,[28] the time evolution of the kth moment can be obtained by multiplying both sides of the aerosol GDE by v_p and by integrating over the particle size range. The result can be written

$$\frac{\partial M_k}{\partial t} = [\dot{M}_k]_{\text{coagulation}} + [\dot{M}_k]_{\substack{\text{surface}\\\text{reactions}}} + [\dot{M}_k]_{\text{nucleation}}. \quad (21)$$

Expressions for each term on the right-hand side of Eq. (21) were obtained based on the detailed derivations of Chiu[29] and of Nijhawan.[30] The first term accounts for the contribution from particle coagulation. For the pressure regime of interest particles are much smaller than the mean free path for collisions in the gas. Thus, free molecule regime expressions were used for the coagulation term. To obtain an analytical form for the coagulation term in the free molecule regime, Lee and Chen[31] introduced a polynomial function, B_k, which is dependent on the geometric standard deviation of particle size distribution, σ_g.

$$B_0 = 0.633 + 0.092\sigma_g^2 - 0.022\sigma_g^3. \quad (22)$$

$$B_2 = 0.39 + 0.5\sigma_g - 0.214\sigma_g^2 + 0.029\sigma_g^3. \quad (23)$$

The final form of the first three coagulation terms is obtained as

$$[\dot{M}_0]_{\text{coagulation}} = -A_1 B_0 (M_{2/3}M_{-1/2} + 2M_{1/3}M_{-1/6}$$
$$+ M_{1/6}M_0), \quad (24)$$

$$[\dot{M}_1]_{\text{coagulation}} = 0, \quad (25)$$

and

$$[\dot{M}_2]_{\text{coagulation}} = 2A_1 B_2 (M_{5/3}M_{1/2} + 2M_{4/3}M_{5/6} + M_1 M_{7/6}), \quad (26)$$

where A_1 is a size-independent variable defined as $A_1 = (3/4\pi)^{1/6}(6k_B T/\rho_p)^{1/2}$, k_B is the Boltzmann constant and ρ_p is particle mass density.

The second term on the right-hand side of Eq. (21), representing particle growth due to surface reactions, can be expressed as

$$[\dot{M}_k]_{\text{growth}} = -\int_0^\infty v_p^k \frac{\partial}{\partial v_p}(Gn(v_p,t))dv_p$$

$$= \int_0^\infty \frac{dv_p^k}{dv_p} Gn(v_p,t)dv_p = k\Psi M_{k-1/3}, \quad (27)$$

where $\psi = G \cdot v_p^{-2/3}$ is independent of particle size, and G is the particle volume growth rate, given by

$$G(v_p) = \frac{(36\pi)^{1/3} v_p^{2/3}}{\rho_p} \sum_{k=1}^{K_b} \dot{s}_k W_k.$$

The homogeneous nucleation term in Eq. (21) can be written as

$$[\dot{M}_k]_{\text{nucleation}} = \int_0^\infty v_p^k J(v_p^*)\delta(v_p - v_p^*)dv_p = (v_p^*)^k J(v_p^*), \quad (28)$$

where δ is the Kronecker delta function and $J(v_p^*)$ is the nucleation rate, which we take to equal the production rate of silicon oxide clusters containing 11 or 12 silicon atoms, calculated from the chemical kinetics model.

The noninteger moments appearing in the above equations can be expressed in terms of the first three integer moments, M_0, M_1 and M_2, by assuming a lognormal size distribution function of the general form

$$n(v_p,t) = \frac{N}{3\sqrt{2\pi}\ln\sigma_g} \exp\left\{-\frac{\ln^2(v_p/\bar{v}_g)}{18\ln^2\sigma_g}\right\} \cdot \frac{1}{v_p}, \quad (29)$$

where N is the total particle concentration. The geometric mean particle volume, $\bar{v}_g$, and the geometric standard deviation, σ_g, can also be expressed in terms of the first three moments by

$$\bar{v}_g = \frac{M_1^2}{M_0^{3/2}M_2^{1/2}}, \quad (30)$$

and

$$\ln^2\sigma_g = \frac{1}{9}\ln\left(\frac{M_0 M_2}{M_1^2}\right). \quad (31)$$

Finally, the kth moment is related to $\bar{v}_g$, σ_g and M_0 by

$$M_k = M_0 \bar{v}_g^{-k} \exp(\tfrac{9}{2}k^2 \ln^2\sigma_g). \quad (32)$$

One thus needs to solve only for the first three moments of Eq. (21), i.e., $k = 0$, 1 and 2, to obtain the value of any arbitrary moment.

In spite of the advantage of moment methods in terms of computational efficiency, it should be noted that the moment equations can potentially cause numerical instabilities, due to the large difference in the relative magnitudes of the moments: $M_0 : M_1 : M_2 \approx 1 \text{ cm}^{-3} : 10^{-15} \text{ cm}^3 \text{ cm}^{-3} : 10^{-30} \text{ cm}^3$ for a 0.1 μm diam particle. Therefore the use of a normalization of the following form is useful:[30]

$$\hat{M}_k = \frac{M_k}{\rho(v_1)^k}, \quad (33)$$

where v_1 is the volume of nuclei and ρ is gas mass density.
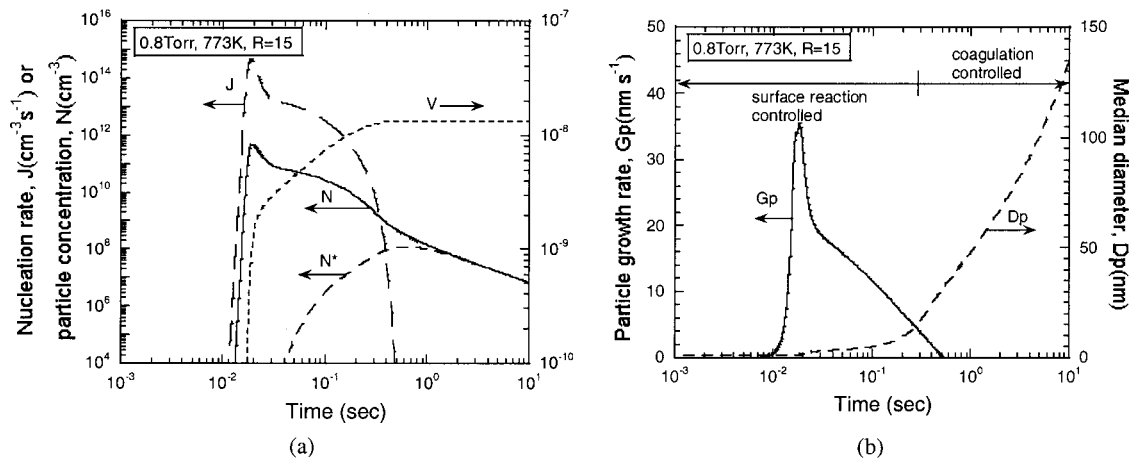
FIG. 4. Predictions of the aerosol dynamics model coupled to the chemical kinetic mechanism at 0.8 Torr, 773 K and $R=15$ in a batch reactor: (a) nucleation rate, J, total particle concentration, N, concentration of particles larger than 50 nm, N^*, and particle volume fraction, V; (b) particle surface growth rate, Gp, and median diameter, Dp.

B. Coagulation enhancement by van der Waals forces

Most models of particle coagulation neglect the effect of interparticle van der Waals forces. However the effect can be significant,[32,33] and we have accounted for it in the present work. Marlow[33] showed that, for water droplets in the free molecule regime, the enhancement in collision rates could range from a factor of 1.01–2.44 depending on the size of the two colliding droplets and the Knudsen number.

In the free molecule regime, the particle flux including the effect of an interaction potential can be written as

$$\Phi_{12} = \Psi_{12} \cdot \tilde{\Phi}_{12}, \tag{34}$$

where Ψ_{12} and $\tilde{\Phi}_{12}$ are, respectively, the correction factor and the flux between particles of radii r_1 and r_2 in the absence of an interaction potential. Marlow's expression[33] is used for the correction factor, Ψ_{12}, which is a function of the radii of the two particles, temperature and the interaction potential for which we adopted Hamaker's formula.[32] A value of 1.8×10^{-12} erg was assumed for the Hamaker constant based on Hamaker's estimate for SiO_2 particles.

Our numerical integration revealed that the correction factor, Ψ_{12}, is a rather insensitive function of the radii of the two collision partners for the conditions of interest. At 773 K, the correction factor, Ψ_{12}, was calculated to vary slightly from 2.6 to 2.8 for particle radii ranging from 0.5 to 100 nm. The calculated values of Ψ_{12} were affected by temperature, ranging from 3.4 to 2.4 as temperatures ranged from 293 to 1273 K. We assumed Ψ_{12} to be radii independent for simplicity of calculation, and obtained a fitting formula in terms of temperature. This correction factor was incorporated into the coagulation terms in Eqs. (22) and (23).

V. RESULTS

The chemical kinetics model coupled to the aerosol dynamics model described above was used to simulate particle nucleation, growth and coagulation during the low-pressure CVD of SiO_2 from silane and oxygen. We conducted zero-dimensional time-dependent calculations in a batch reactor at fixed temperature and pressure. The set of governing equations, Eqs. (15), (20) and (21), must be solved simultaneously because of the cross-coupling terms. We used the differential algebraic sensitivity analysis code (DASAC), a time-dependent algebraic/differential equation solver with the capability of parametric sensitivity analysis.[34] Chemical source terms were evaluated by utilizing the CHEMKIN family of codes.[25] A typical run for a time integration of 10 s required 2 CPU minutes on an SGI Origin 2000 supercomputer.

Figure 4 shows results of these simulations for base case conditions. The production rates of the species with more than 10 silicon atoms, which were assumed to form irreversibly, were summed to give the nucleation rate curve labeled J in Fig. 4(a). J increases very rapidly as the radicals are produced in sufficient concentration to initiate the chain branching reactions at 0.01 s, and peaks at 0.02 s. This initial sharp rise is due to $(SiO_2)_9+(HSiOOH)_2 \rightarrow particle$. However, $(SiO)_{10}+SiO \rightarrow particle$ dominates the subsequent period of nucleation, from 0.03 s until the growth species are completely consumed at 0.5 s. The total concentration of particles, labeled N, closely follows the sharp increase in the nucleation rate, and then declines due to coagulation. Using the calculated standard deviations of the size distribution function, we also determined the concentration of particles with diameters larger than 50 nm, roughly indicative of a critical particle size that within the next few years is predicted to pose a serious contamination problem in semiconductor manufacturing.[2] This filtered concentration, labeled N^*, remains low in the initial stage, where nucleation produces a large number of very small particles, while it approaches the total concentration after 1 s, by which time most of the small particles have undergone coagulation. The particle volume fraction curve is labeled V, which increases
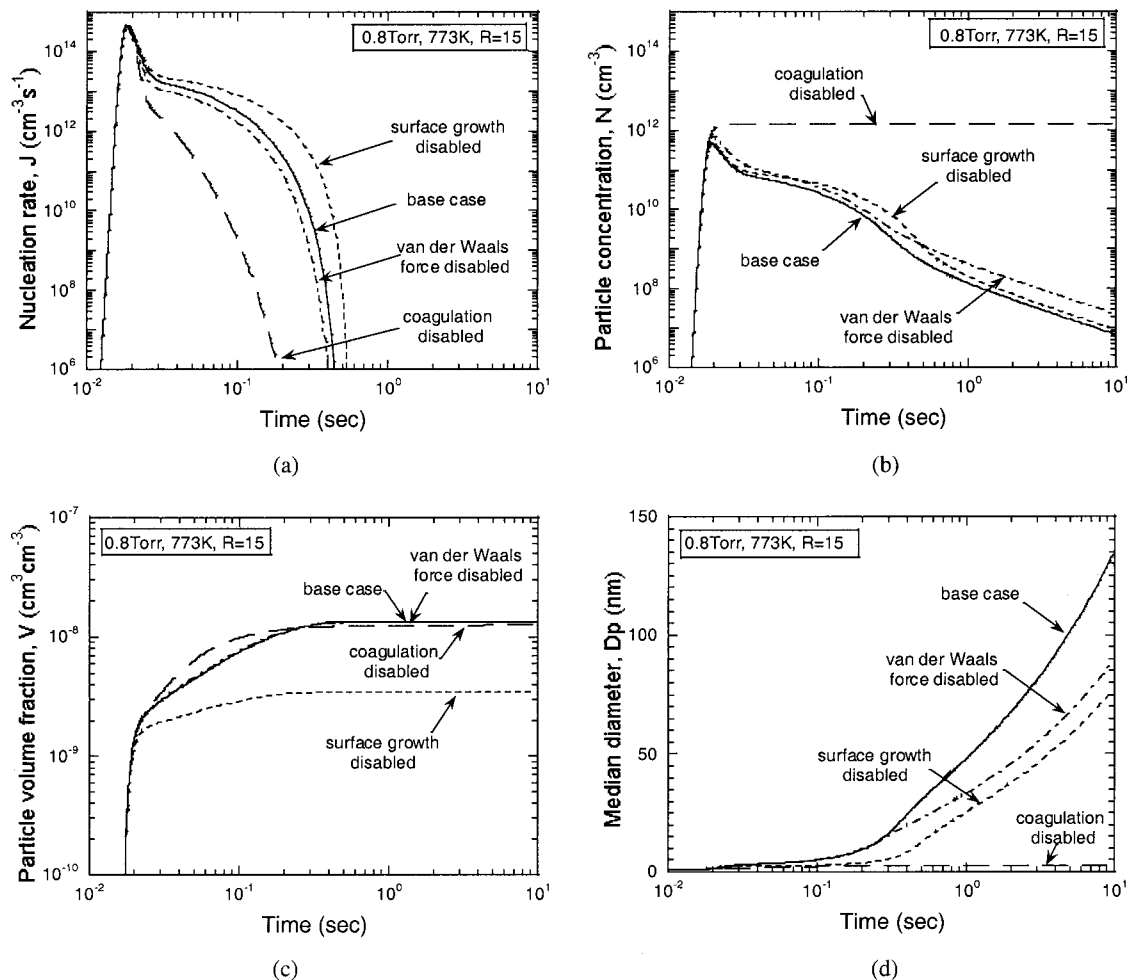
FIG. 5. Effects of particle surface growth, coagulation and van der Waals force: (a) nucleation rates; (b) total particle concentrations; (c) particle volume fractions; (d) particle median diameters.

during the nucleation process and then levels off in the absence of nucleation and surface growth. Since the major gas species contributing to particle surface growth are the two clustering species, SiO and SiO_2, the particle volume fraction barely increases after 0.5 s, because these species have been consumed during the nucleation process.

Figure 4(b) shows the particle surface growth rate curve, labeled Gp, and the particle median diameter curve, labeled Dp. Among the gas species, the two clustering species SiO and SiO_2 are predicted to make the largest contributions to particle surface growth, primarily because these high-concentration species are assigned unity sticking probabilities on the particle surface. It is seen that the particle surface growth rate begins to increase as the concentrations of the two growth species build up at around 0.01 s, and reaches a maximum value of 36 $nm\,s^{-1}$ at 0.02 s. The decrease of the particle surface growth rate after 0.02 s is due to the depletion of the two growth species both by clustering and by surface growth itself. Figure 4(b) reveals a clear division in the particle growth process. During the initial surface-reaction-controlled region, where more surface area is available, the two growth species, SiO and SiO_2, take an active part in surface reactions. After they are consumed, via either

surface reactions or clustering, particle coagulation becomes the only process affecting the particle size and concentration. No new particles are generated, and the median particle size increases rapidly.

Figure 5 shows the predicted effects of surface growth and coagulation. To account for their individual contributions, we disabled each of these processes in turn. Nucleation rates are shown in Fig. 5(a). When surface growth is disabled, more of the growth species are available for clustering, allowing nucleation to persist for a longer time. On the other hand, when coagulation is disabled, more surface area is available for heterogeneous reactions to take place, depleting the species responsible for clustering and thus leading to an earlier cessation of nucleation. Figure 5(b) indicates that coagulation has a large effect on the total concentration of particles, while surface growth has a much smaller effect. After nucleation ceases, the particle concentration remains constant in the case in which coagulation is disabled. The effect of surface growth on particle volume fraction is clearly seen in Fig. 5(c). When surface growth is turned off, the growth species have no route to react on the particle surface, and instead participate only in clustering. The net result is an increase in cluster concentrations in the gas phase and a de-
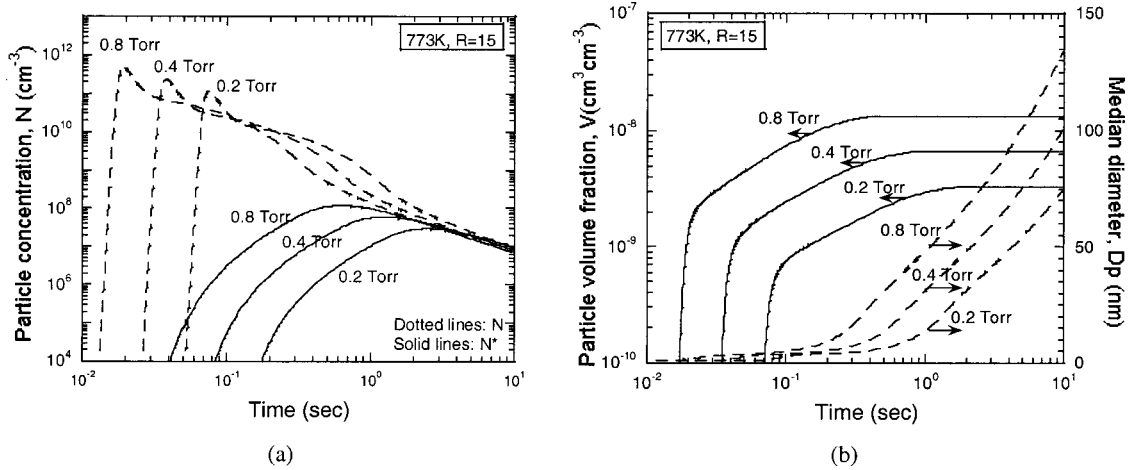
FIG. 6. Effect of pressure on particle dynamics at 773 K and $R = 15$: (a) particle total concentrations and filtered concentrations; (b) particle volume fractions and median diameters.

crease in particle volume fraction. In the base surface mechanism used in this study, a unity sticking probability is assigned for SiO and SiO_2, whereas the other major gas species including HSiOOH and SiH_2O are assumed to be unreactive on a surface.[5] It should be admitted that the assumed surface reactivities of the gas species, which usually involve greater uncertainty compared to gas kinetics, can strongly affect the calculated particle growth. Particle median diameters are compared in Fig. 5(d). When surface growth is disabled, we do not observe as great an increase of the median diameter in the initial stage compared to in the base case. It is also worth noting that particle size barely increases in the absence of coagulation.

In Fig. 6 we examine the effect of varying the pressure from 0.2 to 0.8 Torr. The peaks in the particle concentration curves scale linearly on the pressure—1.2×10^{11}, 2.3×10^{11} and 4.7×10^{11} cm^{-3}, respectively, for 0.2, 0.4 and 0.8 Torr. Pressure also affects the time for the onset of nucleation, resulting from a change in species partial pressure. The time at which the particle concentration peaks scales inversely

with pressure—0.075, 0.038 and 0.019 s for 0.2, 0.4 and 0.8 Torr, respectively. All of the particle concentration curves in Fig. 6(a) are observed to peak and then to reach similar values past 2 s. This asymptotic behavior is explained by self-preserving size distribution theory,[35] which predicts that, for an aerosol undergoing Brownian coagulation in the free molecule regime, $N \propto t^{-6/5}$ and is independent of the initial particle concentration. Although the particle concentration is predicted to reach approximately the same value after about 2 or 3 s regardless of pressure, pressure does strongly affect the particle size and aerosol volume fraction, as seen in Fig. 6(b). The aerosol volume fraction after about 1 s is seen to scale directly on the pressure, i.e., on the initial silane concentration. Smaller particles are produced at lower pressures at any given time, which is a consequence of the strong effect of particle concentration on coagulation rates.

Figure 7 shows the effect of varying the temperature from 573 to 773 K. At 573 K, as seen in Fig. 7(a), the particle concentration at 10 s remains higher than in the other cases shown by two orders of magnitude. This result is attribut-
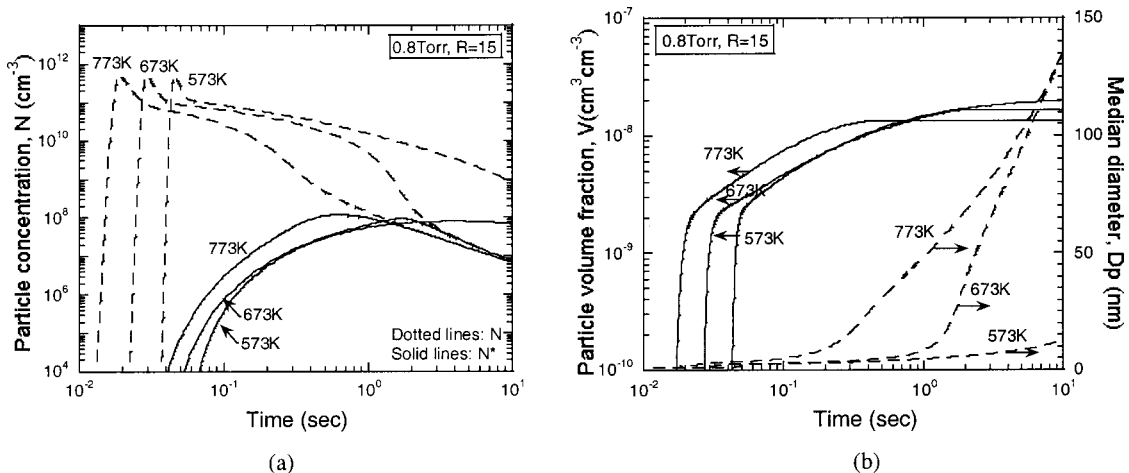

FIG. 7. Effect of temperature on particle dynamics at 0.8 Torr and $R = 15$: (a) total particle concentrations and filtered concentrations; (b) particle volume fractions and median diameters.

able, in large part, to the chain-propagating reaction, $SiO+O_2 \rightarrow SiO_2+O$. At low temperatures, this route becomes practically shut off and more SiO becomes available for clustering reactions. As a result, nucleation persists for a longer time, keeping the median diameter of particles below 15 nm. Particle volume fractions are predicted to be slightly larger at lower temperatures, since the extended nucleation time at a lower temperature allows more surface area for particle growth. It is also interesting to note in Figs. 4–7 that the leveling off of the volume fraction curves coincides with an inflection point in the median diameter curves. This is consistent with the explanation made above of the two growth regimes, surface reaction controlled and coagulation controlled.

VI. SUMMARY

A detailed kinetic model has been developed for silicon oxide clustering that leads to particle nucleation during low-pressure silane oxidation. QRRK theory was applied to an existing silane oxidation mechanism to estimate the pressure dependence of a number of unimolecular reactions. Four classes of clustering pathways were considered based on current knowledge of reaction kinetics and cluster properties. The species conservation equations and a moment-type aerosol dynamics model were formulated for a batch reactor undergoing particle nucleation, surface growth and coagulation. The chemical kinetics model was coupled to the moment model to predict particle dynamics. Time-dependent zero-dimensional simulations were conducted to assess the effects of the contributing processes, and of temperature and pressure.

The dominant reactions that formed ''particles'' in our mechanism were found to be $(SiO_2)_9+(HSiOOH)_2 \rightarrow particle$ and $(SiO)_{10}+SiO \rightarrow particle$. SiO and SiO_2 are also predicted to play an important role in particle surface growth. The particle growth process is characterized by two distinct regimes: an initial surface-reaction-controlled regime where the particle volume fraction increases due to nucleation and surface reactions, and a subsequent coagulation-controlled regime where coagulation leads to a rapid increase in particle size and therefore to a gradual decrease in particle concentration. Pressure affects the nucleation process mainly through a change in precursor partial pressures, whereas temperature affects nucleation through changes in reaction rate constants.

APPENDIX: ESTIMATED CLUSTER THERMOCHEMICAL PROPERTIES

TABLE III. Polynomial fitting coefficients for clusters in the standard NASA format.

Species	a_1	a_2	a_3	a_4	a_5	a_6	a_7
SiO	3.709 1712$E+00$	9.069 7284$E+04$	-4.233 0473$E-07$	9.034 4073$E-11$	-7.280 2576$E-15$	-1.349 4045$E+04$	3.184 2188$E+00$
Si_2O_2	9.762 5847$E+00$	-1.593 5308$E-04$	2.318 0722$E-07$	-7.572 0988$E-11$	7.771 6860$E-15$	-5.337 1079$E+04$	-2.302 1760$E+01$
Si_3O_3	1.561 3486$E+01$	-2.211 6911$E-04$	3.452 3671$E-07$	-1.139 6278$E-10$	1.174 1059$E-14$	-9.507 0114$E+04$	-4.974 6628$E+01$
Si_4O_4	2.115 7012$E+01$	2.073 9416$E-04$	1.799 4268$E-07$	-8.450 1387$E-11$	9.740 7392$E-15$	-1.283 1132$E+05$	-7.056 0939$E+01$
Si_5O_5	2.619 1211$E+01$	1.333 8465$E-03$	-3.282 7956$E-07$	1.749 2749$E-11$	2.154 3416$E-15$	-1.685 0283$E+05$	-8.829 9259$E+01$
Si_6O_6	3.185 1958$E+01$	1.502 8756$E-03$	-3.012 5048$E-07$	-1.051 5966$E-11$	6.134 5351$E-15$	-2.069 4060$E+05$	-1.097 0323$E+02$
Si_7O_7	3.751 2704$E+01$	1.671 9046$E-03$	-2.742 2140$E-07$	-3.852 4681$E-11$	1.011 4729$E-14$	-2.453 7937$E+05$	-1.311 0721$E+02$
Si_8O_8	4.317 3451$E+01$	1.840 9336$E-03$	-2.471 9233$E-07$	-6.653 3396$E-11$	1.409 4922$E-14$	-2.838 0506$E+05$	-1.525 1118$E+02$
Si_9O_9	4.883 4197$E+01$	2.009 9626$E-03$	-2.201 6325$E-07$	-9.454 2112$E-11$	1.807 5115$E-14$	-3.222 6095$E+05$	-1.739 1515$E+02$
$Si_{10}O_{10}$	5.449 4944$E+01$	2.178 9916$E-03$	-1.931 3418$E-07$	-1.225 5083$E-10$	2.205 5309$E-14$	-3.607 0173$E+05$	-1.953 1913$E+02$
SiO_2	6.209 0534$E+00$	1.363 1043$E-03$	-5.942 2051$E-07$	1.199 1553$E-10$	-9.228 2308$E-15$	-3.554 8797$E+04$	-8.428 7447$E+00$
Si_2O_4	1.412 4110$E+01$	1.595 0164$E-03$	-5.422 0059$E-07$	8.203 2840$E-11$	-4.467 7341$E-15$	-1.153 2942$E+05$	-4.543 5969$E+01$
Si_3O_6	2.245 9020$E+01$	1.917 3620$E-03$	-5.322 1537$E-07$	5.317 4897$E-11$	-4.433 4868$E-16$	-2.005 4665$E+05$	-8.854 1520$E+01$
Si_4O_8	3.078 9209$E+01$	2.250 4993$E-03$	-5.288 5450$E-07$	2.594 2087$E-11$	3.439 3352$E-15$	-2.851 2765$E+05$	-1.293 2230$E+02$
Si_5O_{10}	3.911 1755$E+01$	2.592 8812$E-03$	-5.302 7648$E-07$	-1.378 3655$E-13$	7.217 4148$E-15$	-3.698 2254$E+05$	-1.709 5038$E+02$
Si_6O_{12}	4.738 5779$E+01$	3.015 7212$E-03$	-5.799 7804$E-07$	-1.383 0300$E-11$	9.844 7246$E-15$	-4.543 8869$E+05$	-2.122 4988$E+02$
Si_7O_{14}	3.796 7736$E+01$	3.322 2336$E-02$	-1.876 2707$E-05$	4.700 9253$E-09$	-4.329 1249$E-13$	-5.295 9089$E+05$	-1.532 0877$E+02$
Si_8O_{16}	3.753 4746$E+01$	4.833 1588$E-02$	-2.777 2963$E-05$	7.028 6348$E-09$	-6.512 3762$E-13$	-6.096 5897$E+05$	-1.451 4804$E+02$
Si_9O_{18}	3.710 1755$E+01$	6.344 0840$E-02$	-3.678 3218$E-05$	9.356 3443$E-09$	-8.695 6276$E-13$	-6.897 2705$E+05$	-1.370 8732$E+02$
$Si_{10}O_{20}$	3.666 8764$E+01$	7.855 0092$E-02$	-4.579 3473$E-05$	1.168 4054$E-08$	-1.087 8879$E-12$	-7.697 9513$E+05$	-1.290 2659$E+02$
$(SiH_2O)_2$	1.397 2585$E+01$	7.488 1421$E-03$	-2.920 5751$E-06$	5.324 9786$E-10$	-3.733 7067$E-14$	-8.528 3138$E+04$	-4.999 5569$E+01$
$(HSiOOH)_2$	1.951 4769$E+01$	6.427 4929$E-03$	-2.005 8889$E-06$	2.817 5472$E-10$	-1.416 0852$E-14$	-1.765 0975$E+05$	-7.454 5852$E+01$

The specific heat capacity at constant pressure, C_p°, the standard-state enthalpy, H°, and the standard-state entropy, S°, respectively, are defined as follows:

$$\frac{C_p^\circ}{R} = a_1 + a_2 T + a_3 T^2 + a_4 T^3 + a_5 T^4,$$

$$\frac{H^\circ}{RT} = a_1 + \frac{a_2}{2} T + \frac{a_3}{3} T^2 + \frac{a_4}{4} T^3 + \frac{a_5}{5} T^4 + \frac{a_6}{T},$$

and

$$\frac{S^\circ}{R} = a_1 \ln T + a_2 T + \frac{a_3}{2} T^2 + \frac{a_4}{3} T^3 + \frac{a_5}{4} T^4 + a_7,$$

where R is the universal gas constant and T is the gas temperature in K. These coefficients are valid only for the gas temperature ranging from 300 to 1500 K.

[1] S. A. Campbell, *The Science and Engineering of Microelectronic Fabrication*, 1st ed. (Oxford, New York, 1996).

[2] *The National Technology Roadmap for Semiconductors* (Semiconductor Industry Association, San Jose, CA, 1997).

[3] H. J. Emeleus and K. J. Stewart, Chem. Soc. **1935**, 1182 (1935).

[4] V. I. Babushok, W. Tsang, D. R. Burgess, Jr., and M. R. Zachariah, *Twenty-seventh Symposium (International) on Combustion* (The Combustion Institute, University of Colorado at Boulder, 1998), p. 2431.

[5] E. Meeks, R. S. Larson, P. Ho, C. Apblett, S. M. Han, E. Edelberg, and E. S. Aydil, J. Vac. Sci. Technol. A **16**, 544 (1998).

[6] M. Liehr and S. A. Cohen, Appl. Phys. Lett. **60**, 198 (1992).

[7] M. T. Swihart and S. L. Girshick, J. Phys. Chem. B **103**, 64 (1999).

[8] S. L. Girshick, M. T. Swihart, S.-M. Suh, M. R. Mahajan, and S. Nijhawan, J. Electrochem. Soc. **147**, 2303 (2000).

[9] D. Lindackers, M. G. D. Strecker, P. Roth, C. Janzen, and S. E. Pratsinis, Combust. Sci. Technol. **123**, 287 (1997).

[10] E. Whitby and M. Hoshino, J. Electrochem. Soc. **143**, 3397 (1996).

[11] M. R. Zachariah, Chem. Eng. Sci. **45**, 2551 (1990).

[12] T. Kudo and S. Nagase, J. Am. Chem. Soc. **107**, 2589 (1985).

[13] M. R. Zachariah and W. Tsang, Aerosol. Sci. Technol. **725**, 1560 (1993).

[14] M. R. Zachariah and W. Tsang, J. Phys. Chem. **99**, 5308 (1995).

[15] S. K. Nayak, B. K. Rao, S. N. Khanna, and P. Jena, J. Chem. Phys. **109**, 1245 (1998).

[16] A. M. Dean, J. Phys. Chem. **89**, 4600 (1985).

[17] P. R. Westmoreland, J. B. Howard, J. P. Longwell, and A. M. Dean, AIChE J. **32**, 1971 (1986).

[18] P. R. Westmoreland, Combust. Sci. Technol. **82**, 151 (1992).

[19] K. A. Holbrook, M. J. Pilling, and S. H. Robertson, *Unimolecular Reactions* (Wiley, New York, 1996).

[20] D. M. Golden, R. K. Solly, and S. W. Benson, J. Phys. Chem. **75**, 1333 (1971).

[21] J. A. Britten, J. Tong, and C. K. Westbrook, *Twenty-third Symposium (International) on Combustion* (The Combustion Institute, University of Orlans, France, 1990), p. 195.

[22] A. E. Lutz, R. J. Kee, and J. A. Miller, Sandia National Laboratories Report No. SAND87-8248, Albuquerque, NM (1988).

[23] P. Ho, M. E. Coltrin, and W. G. Breiland, J. Phys. Chem. **98**, 10138 (1994).

[24] D. A. McQuarrie, *Statistical Mechanics* (Harper & Row, New York, 1976).

[25] R. J. Kee, F. M. Rupley, E. Meeks, and J. A. Miller, Sandia National Laboratories Report No. SAND96-8216, Albuquerque, NM (1996).

[26] M. E. Coltrin, R. J. Kee, F. M. Rupley, and E. Meeks, Sandia National Laboratories Report No. SAND96-8217, Albuquerque, NM (1996).

[27] J. Appel, H. Bockhorn, and M. Frenklach, Combust. Flame **121**, 122 (2000).

[28] S. E. Pratsinis and K.-S. Kim, J. Aerosol Sci. **20**, 101 (1989).

[29] C.-P. Chiu, Ph.D. dissertation, University of Minnesota, 1992.

[30] S. Nijhawan, Ph.D. dissertation, University of Minnesota, 1999.

[31] K. W. Lee and H. Chen, Aerosol. Sci. Technol. **3**, 327 (1984).

[32] M. K. Alam, Aerosol. Sci. Technol. **6**, 41 (1987).

[33] W. H. Marlow, J. Chem. Phys. **73**, 6288 (1980).

[34] M. Caracotsios and W. E. Stewart, Comput. Chem. Eng. **9**, 359 (1985).

[35] S. K. Friedlander, *Smoke, Dust and Haze: Fundamentals of Aerosol Behavior* (Wiley, New York, 1977).